# Smart Plug 2.0: A Solid-State Smart Plug Device Preventing Fire and Shock Hazards

Zhixi Deng, *Member, IEEE*, Yuanfeng Zhou, *Member, IEEE*, Ahmad Kamal, *Member, IEEE*, Risha Na, *Member, IEEE*, Ian P. Brown, *Senior Member, IEEE*, and Z. John Shen, *Fellow, IEEE*

***Abstract*—Electrical faults cause fire or shock hazards in homes and offices. Flexible power cords are particularly susceptible to metal or insulation degradation that may lead to a variety of electrical faults. This article introduces a new Smart Plug 2.0 device which offers all-in-one protection against short-circuit, overload, arc, and ground faults in addition to the wireless power control and monitor function of conventional smart plug devices. It offers microsecond-scale time resolution to detect and respond to a fault condition, and significantly reduces the electrothermal stress on household electrical wires and loads. A new arc fault detection method is developed using machine learning models based on load current *di/dt* events. Comparing to other solid-state circuit breaker designs which typically respond to overcurrent conditions only, Smart Plug 2.0 integrates additional protective functions into the same hardware structure with minimal cost penalty. A 120 V/10 A solid-state Smart Plug 2.0 prototype using power MOSEFTs is designed and tested. It has experimentally demonstrated the comprehensive protection features against all types of electrical faults.**

***Index Terms*—Arc fault detection, circuit fault, machine learning, smart plug, solid state circuit breaker.**

## I. Introduction

IT IS estimated by the National Fire Protection Association that 44 880 residential electrical fires occurred between 2012 and 2016, resulting in 440 deaths, $1.3 billion in property damages, and 1250 injuries on average per year in the U.S. [1]. Approximately half of the residential electrical fires involve some form of arcing faults. An arc fault occurs in degraded or damaged power cords or electrical connections. When a partial disconnection between strand wires and connectors causes a high resistance hot spot which carbonizes the insulating materials, a series arc is formed on the carbonized path. The center of the arc can reach a temperature well over 5000°C and ignite the surrounding materials [2].

Manuscript received 5 August 2022; accepted 9 November 2022. Date of publication 29 November 2022; date of current version 26 December 2022. This work was supported in part by the Advanced Research Projects Agency-Energy, U.S. Department of Energy, under Grant DE-AR0000890 in the CIRCUITS program monitored by Dr. Isik Kizilyalli. Recommended for publication by Associate Editor S. Williamson. *(Corresponding author: Zhixi Deng.)*

The authors are with the Electrical and Computer Engineering, Illinois Institute of Technology, IL Chicago 60616 USA (e-mail: zdeng6@hawk.iit.edu; yzhou103@hawk.iit.edu; akamal1@hawk.iit.edu; rna@iit.edu; ibrown1@iit.edu; zshen6@iit.edu).

Color versions of one or more figures in this article are available at https://doi.org/10.1109/TPEL.2022.3224483.

Digital Object Identifier 10.1109/TPEL.2022.3224483

Ground faults caused by degraded or broken insulating materials between the line and ground wires are another type of electrical faults that can cause shock hazards, resulting in roughly 500 deaths in the U.S. each year [3]. A short-circuit fault between the line and neutral wires is yet another type of electrical faults that result in excessive fault currents (10–30 times of nominal current) and potentially fire hazards if not protected properly [4]. An overload fault is similar to a short circuit fault, but usually at a lower fault current level (several times of nominal current). It is worth noting the difficulty to distinguish between an overload fault current and a normal overcurrent scenario such as inrush and motor starting surge current.

Overcurrent protection in homes and offices, including short circuit and overload protection, is provided by molded case circuit breakers (MCCBs) based on thermal, thermal-magnetic, hydraulic magnetic, or magnetic tripping mechanisms in the power main panel boxes [4]. Different time-current response curves are provided based on the application to react to fault conditions while accommodating normal inrush currents. Ground fault circuit interrupters (GFCIs) for residential use are the most effective way to prevent deadly electric shocks. A GFCI protects personnel by interrupting the ground leakage circuit when a current to ground exceeds 4–6 mA [5]. Arc fault circuit interrupters (AFCIs) interrupt the circuit when the presence of dangerous electrical arcs is detected, while avoiding nuisance tripping of electric arcs generated by normal load operation (relay switches, electrical power tools, motors, etc.). Combination type of GFCI or AFCI circuit breakers start to come into the market in recent years. However, their installation is currently limited to newly constructed or renovated homes, which count only 1% of all the homes in the U.S. [2].

In comparison to fixed wirings in homes and offices, flexible power cords plugged into wall receptacles are subject to more mechanical stress and fatigue and are more susceptible to degradation of insulating materials and conducting metal wires. A common example is the repeatedly overstretched power cords of laptop computers. This may result in two scenarios: breakdown of wire insulation or partial disconnection of strand wires. A bad insulation between line and neutral or line and ground can cause short circuit faults. Even more dangerously, ground faults (broken line to ground insulation) or series arc faults (intermittently broken line or neutral wire) can happen, which are not protected by the conventional upstream MCCB due to their low fault current levels. A ground fault can cause dangerous

Fig. 1. Examples of Smart Plug 1.0 products.

shock hazards while an arc fault is a major cause of fire hazards. According to the Electrical Safety Foundation International, roughly 3300 home fires and 50 deaths originate from faulty power cords in the U.S. alone each year [3]. Considering the vast number of consumer products and the power cords used with them worldwide, it would be highly impactful to develop a protective solution at the wall outlet to provide protection against all sorts of electrical faults on the plug-in power cords. This would be particularly beneficial for 99% of the homes and offices which do not have AFCI or GFCI to cover every single wall receptacle.

Recently, Smart Plug products (referred to as Smart Plug 1.0 in this article) are becoming increasingly popular in the consumer market with a global revenue growing from $710M in 2016 to $2.59B in 2021 [6]. Smart Plug 1.0 offers an affordable and user-friendly way to transform ordinary home appliances, lighting, and any other residential electrical loads into smart home devices, enabling remote control, energy management, or demand response [7]. It currently uses an electromechanical relay to connect or disconnect a load from a power outlet via Wi-Fi communication and control [8]. It can easily enable demand response, which changes the normal consumption patterns in electricity use by end-users in response to changes in the price of electricity over time, so that utility companies can directly control some of the non-time-critical home appliances (e.g., washer/dryers and refrigerators) depending on the real-time power demand and supply [9]. Demand response is generally considered an effective and easy-to-implement approach to reduce fossil fuel consumption and carbon emission. Numerous manufacturers around the world offer Smart Plug 1.0 products, as shown in Fig. 1.

Smart Plug devices would be an ideal vehicle for realizing the aforementioned fault protection for the plug-in power cords and loads. However, none of the existing Smart Plug 1.0 products offers such protective features, largely because the electromechanical relay is not capable of interrupting a large fault current. Tens of milliseconds will pass before the upstream circuit breaker can shut down the power supply, during which time the smart plug itself, the load appliance, the power cord, and the house wiring system must endure a very stressful fault current (hundreds of amperes or higher), a scenario both dangerous and detrimental to the properties and occupants. When the upstream circuit breaker (CB) eventually trips, all other non-fault outlets on the same branch would lose power, resulting in an annoying situation in residential homes and a major disturbance and loss of productivity in offices.

The purpose of this article is to develop a solid-state smart plug device (termed Smart Plug 2.0 in this article) that provides all-in-one protection against short circuit, overload, ground, and arc faults, and prevents fire and shock hazards in homes and offices in addition to the common smart features of Smart Plug 1.0 [10]. The authors reported the basic concept of Smart Plug 2.0 in [11], but this article further expands the work scope with new results, particularly related to arc fault detection and protection. It should be mentioned that some prior work in the literature proposed to replace the mechanical relays of Smart Plug devices with thyristors to realize a dimmer-like power control function [12], [13], but none investigated any fault protection options so far. In comparison to other solid-state circuit breakers (SSCBs) which typically react to an overcurrent condition, Smart Plug 2.0 integrates additional important protective functions, such as arc and ground fault protection, into the same hardware design with a minimal cost penalty.

The remainder of this article is organized as follows. Section II introduces the basic concept and hardware design of Smart Plug 2.0. Section III discusses the protection control strategy, including overcurrent, and ground fault. Section IV presents a machine-learning based arc fault detection strategy. Section V demonstrates the experimental results. Discussion and conclusion remarks are presented in Section VI.

## II. Basic Concept and Design

The main advantages of the new Smart Plug 2.0 include all-in-one protection functions, ultrafast response time (microsecond-scale), and low overcurrent (only 2–3 times of nominal current) stress on wires and loads. In addition, Smart Plug 2.0 can distinguish between arc from normal load operation (e.g., relay switching or brushed dc motor) and dangerous arc faults, using a new machine learning based arc fault detection method. Furthermore, Smart Plug 2.0 can also distinguish between a normal inrush current during load startup and a true short circuit fault current even though both exceed the preset overcurrent threshold. Table I gives the functionality comparison of Smart Plug 2.0, Smart Plug 1.0, and commercial circuit breaker, GFCI, or AFCI products. Beside the basic smart functions, Smart Plug 2.0 offers all-in-one protection against shock or fire hazards that are not available in Smart Plug 1.0 devices. Smart Plug 2.0 offers smart communication and control functions that are not offered by commercial CB/GFCI/AFCI products. Furthermore, Smart Plug 2.0 uses power MOSFETs instead of a mechanical relay to switch the load current, thus can respond to a fault in microseconds instead of tens of milliseconds as in the other two cases. This results in significantly reduced fault current stress on the wiring systems, receptacles, and loads. For example, Smart Plug 2.0 is designed to limit the fault or inrush current to 2–3 times of the nominal current rating, while the conventional

TABLE I
COMPARISON OF SMART PLUG 2.0, SMART PLUG1.0, AND COMMERCIAL CIRCUIT BREAKER/GFCI/AFCI PRODUCTS

| Function | Smart Plug 1.0 [6] | Commercial Circuit Breaker/GFCI/AFCI | Smart Plug 2.0 |
|---|---|---|---|
| Wi-Fi control | Yes | Some | Yes |
| Smart power metering | Yes | Some | Yes |
| Switching device | Mechanical | Mechanical | Power MOSFET |
| Response time | ms | ms | μs |
| Overcurrent stress | >10X nominal | >10X nominal | 3X nominal |
| Short circuit protection | No | Yes | Yes |
| Overload protection | No | Yes | Yes |
| Arc fault protection | No | Yes (AFCI) | Yes |
| Ground fault protection | No | Yes (GFCI) | Yes |
| Protection coverage | N/A | After panel box | After outlet |
| Fault locating and isolation | N/A | Difficult (entire branch) | Easy (plug-in power cord) |
| Surge protection | Some | No | Yes |

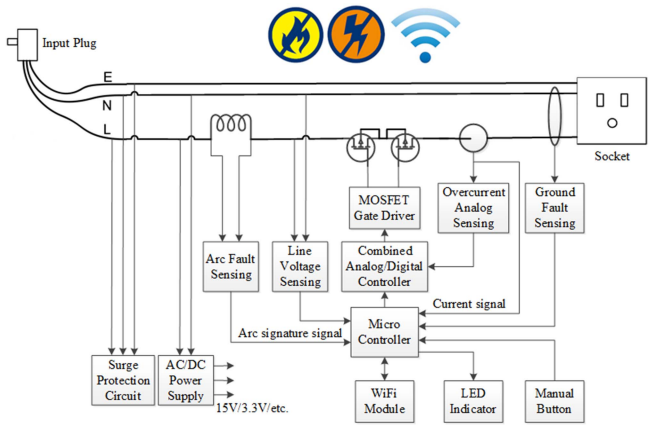


Fig. 2. Conceptual block diagram of Smart Plug 2.0.

circuit breaker in the power panel box trips at 20–30 times of the nominal current rating [14].

Fig. 2 shows a conceptual block diagram of Smart Plug 2.0 hardware design. It comprises an input plug for connecting to an electrical outlet, an electrical socket for a power cord to plug in, a Wi-Fi module for receiving and transmitting data, and a microcontroller for controlling the circuit operation based on wireless communications and sensor signals. The microcontroller is programmed with control algorithms to be described in Section III.

Smart Plug 2.0 uses two back-to-back connected silicon power MOSFETs as a bidirectional switch to control the current flow from the outlet to the load along with a MOSFET gate driver integrated circuit. A Hall effect current sensor is used to monitor the load current and detect any overcurrent conditions. It constantly sends the current sensing signal to the analog-digital-converter (Adc) port of the microcontroller for the control algorithms. At the same time, the sensing signal is also constantly monitored by a fast-acting overcurrent analog sensing circuit, which generates a microsecond-scale fast overcurrent fault signal. This signal is sent to a combined analog/digital controller circuit when the load current exceeds a preset threshold (e.g., twice the nominal current) without waiting for the relatively slow digital control signal from the microcontroller. The combined analog/digital controller uses a simple flip-flop logic circuit to latch the overcurrent fault signal and rapidly turns OFF the power MOSFETs. Then, the microcontroller will authenticate the overcurrent condition and determine whether the overcurrent condition results from an inrush current or a true short-circuit fault. If it is deemed to be an inrush current, the power MOSFETs will turn back ON again. If it is deemed to be a short circuit fault, the MOSFETs will stay off. This hybrid analog/digital control method combines the fast response of analog control and flexibility of digital control [15], [16] and offers an excellent solution for the Smart Plug 2.0 application.

A ground fault current sensor (i.e., a differential current transformer) and a corresponding analog detection circuit are used to sense the ground leakage current and generate a ground fault control signal for the microcontroller. A resistor voltage divider differential amplifier circuit is used to measure the ac line voltage, which is sent to the Adc port of the microcontroller for power metering measurements and the detection of voltage zero crossing for the control algorithms. A voltage surge protection circuit is also included to suppress voltage surges across the wires. Several isolated ac/dc and dc/dc power converters are used to input power from the ac wires and provide +3.3 V and +5 V for the sensors and control circuits, and +15 V for the MOSFET gate driver. A capacitive touch button is used to send a manual control signal to the microcontroller to turn ON and OFF or reset the Smart Plug 2.0 device, and a dual LED indicator is used to indicate the operating status. Note that all the protective functions are implemented by sharing the same basic hardware platform, including the power MOSFETs, microcontroller, current sensors, and auxiliary power supply.

## III. FAULT PROTECTION STRATEGY

In this section, the circuit fault protection strategies are discussed. To illustrate the control architecture and strategies, program flowcharts are used, which would be explained in detail. The top-level program architecture is explained, followed by each fault protection feature, including short circuit fault, overload fault, and ground fault.

### A. Control Architecture

The top-level control program is responsible for the initialization of Smart Plug 2.0 upon powering on. It starts when the Smart Plug 2.0 is powered up. The microcontroller starts with a system initialization program, then enables timer interrupt. It is followed by an infinite loop which does not terminate until the Smart Plug 2.0 is reset or powered off. In the meantime, a main program responsible for the operation of Smart Plug 2.0 runs periodically. As illustrated in Fig. 3, the timer interrupt program starts running with a fixed cycle time of 48 $\mu$s, which is longer than the maximum execution time of the timer interrupt program. The program first starts Adc conversion and reads all GPIO states. Next, the microcontroller waits for the ADCs to complete conversion by polling Adc data, then processes the

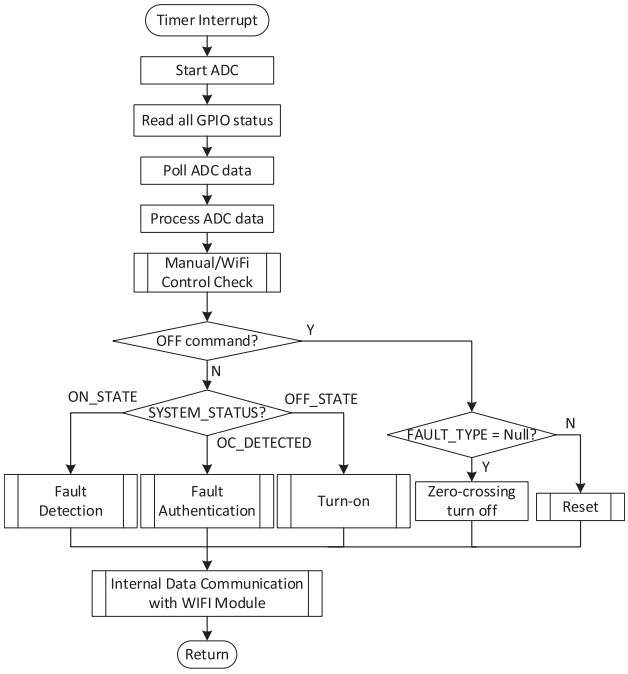


Fig. 3. Timer interrupt program flowchart.

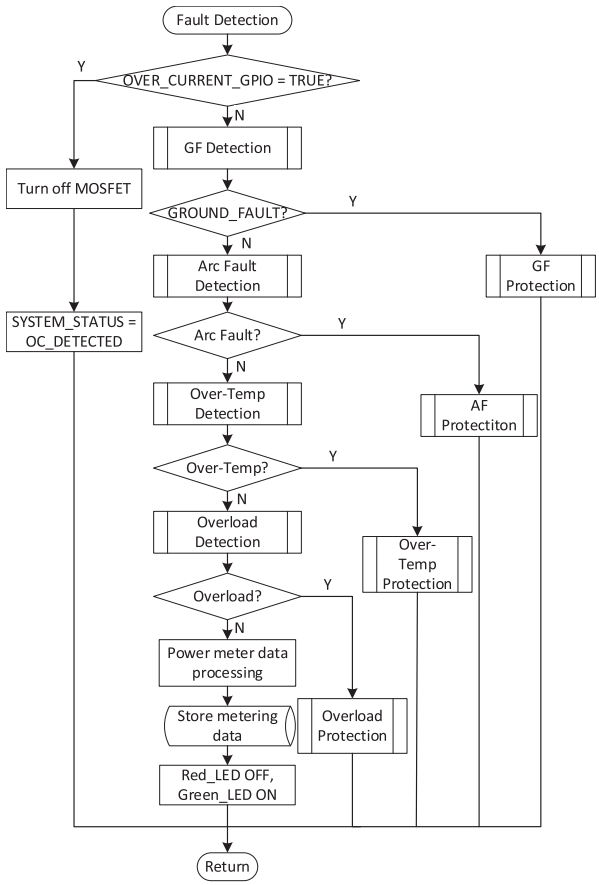


Fig. 4. Fault detection program flowchart.

data. The timer interrupt program then checks the Wi-Fi or manual control command signal. If it receives an off command, it will branch into a turn-OFF program. If the Smart Plug 2.0 has already detected a fault and the MOSFETs are OFF, the capacitive touch button can reset the system. Otherwise, it will turn OFF the MOSFETs at the next line voltage zero crossing. Then, the program continues to read the SYSTEM_STATUS flag. If the SYSMTEM_STATUS flag shows an off-state (OFF_STATE flag) from the previous interrupt cycle, the program will branch into a turn-ON program. If the SYSMTEM_STATUS flag shows an on-state (ON_STATE flag) from the previous interrupt cycle, the program will branch into a fault detection program. If the SYSMTEM STATUS flag shows that an overcurrent condition has been detected (OC_DETECTED) from the previous interrupt cycle, the program will branch into a short circuit fault authentication program. All the branch programs will return to an internal data communication program to communicate with the Wi-Fi module before exiting the timer interrupt program. Finally, the timer interrupt program returns to the infinite loop in the main program and waits for the next timer interrupt to restart the program. Since ac line voltage and load current are sampled every 48 $\mu$s by the periodic interrupt program, Smart Plug 2.0 has much higher time resolution than a typical Smart Plug 1.0.

Various fault protection programs run in sequence, such as overcurrent, ground, arc, overtemperature, and overload faults protection. Fig. 4 illustrates a conceptual fault detection program flowchart of Smart Plug 2.0. The sequence is based on the priority level of each fault. The highest priority is overcurrent protection. The OVER_CURRENT_GPIO signal indicates that the hardware instantaneous trip has occurred, and software protection would take over. The program will turn OFF the MOSFETs immediately upon detecting an overcurrent condition by the current sensor and set the SYSMTEM_STATUS flag to OC_DETECTED. Otherwise, it will go through other fault detection programs one after another, and branch into a corresponding protection program if a particular fault is detected. Ground fault detection has a response time of half ac cycle (8.33 ms); therefore, it has second priority. Arc fault detection follows since it has a response time of 0.5 s. Next is over-temperature detection, which has a response time of tens of seconds. The lowest priority is overload fault detection, since it has a response time of tens of seconds to minutes, depending on the tripping curve. After going through all the fault detection programs, the power metering data will be processed and stored, and the LED indicators will be refreshed before returning to the timer interrupt program if no fault is detected.

### *B. Overcurrent Faults Protection Strategy*

An overcurrent condition can be caused by a short circuit, inrush startup, or overload. The analog overcurrent protection circuit of Smart Plug 2.0 responds to a short circuit or inrush overcurrent nondiscriminatively. After the initial shutdown response, it is up to a short circuit fault authentication program to distinguish between a true short circuit fault and a normal inrush

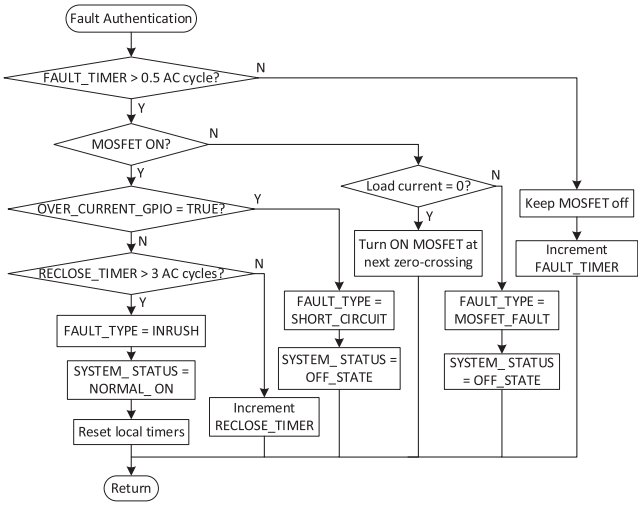


Fig. 5. Short-circuit fault authentication program flowchart.

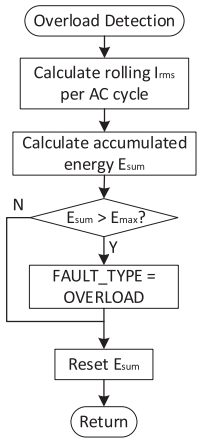


Fig. 6. Overload fault detection program flowchart.

current condition occurred during load startup, as illustrated in Fig. 5. The power MOSFETs will be instantly turned OFF once an overcurrent condition is detected by the overcurrent analog control circuit but will be turned back on ("reclosed") again after a full half ac cycle (roughly 8.3 ms) at the next ac voltage zero crossing by this program to authenticate the fault. If it is deemed a true short circuit fault, it will turn OFF the MOSFETs permanently and set the SYSMTEM_STATUS flag to OFF_STATE and the FAULT_TYPE flag to SHORT_CIRCUIT. If it is deemed to be an inrush current case, the MOSFETs will continue to conduct until the current exceeds the overcurrent threshold again. This inrush current charging process may repeat until the MOSFETs turn ON permanently and the SYSMTEM_STATUS flag is set to NORMAL_ON and the FAULT_TYPE flag set to INRUSH. However, if the MOSFETs are damaged after interrupting a short circuit current, the system goes into OFF_STATE and the FAULT_TYPE flag will be set to MOSFET_FAULT. Then, the upstream circuit breaker would trip. Note that the reclosing action is designed to occur at the next ac voltage zero-crossing to charge the load capacitor from 0 V to minimize the inrush charging current, and to reduce the overcurrent stress on the Smart Plug 2.0 and the wiring system.

Fig. 6 illustrates an overload fault detection program flowchart. It is responsible for detecting a fault condition in which the accumulated transmitted energy over a preset rolling time window exceeds a certain preset value (e.g., 125% of the nominal power rating for 1 second) while the instantaneous current is still below the preset overcurrent threshold (2–3 times nominal current). Using Joule's Law, the normalized electric energy $Q_{\rm sum}$ transferred over a preset rolling window is expressed as

$$Q_{\rm sum} = \int_{t_0}^{t_{\rm window}} i_{\rm load}^2 dt \tag{1}$$

where $\rm i_{load}$ is the load current and $t_{\rm window}$ is the preset rolling time window. The actual thermal energy dissipated on the wiring or load can be easily calculated by multiplying $Q_{\rm sum}$ by the respective resistance value.

The overload threshold $Q_{\rm max}$ can be expressed as

$$Q_{\rm max} = (aI_{\rm rated})^2 t_{\rm window} \tag{2}$$

where $I_{\rm rated}$ is the nominal load current rating, $a$ is a safety margin factor typically in a range of 1.0–1.5. The wiring system can usually sustain a load current slightly higher than its nominal rating for a short period of time. However, under no circumstances should the accumulated $Q_{\rm sum}$ over any rolling time window exceed $Q_{\rm max}$ to ensure the safety of the entire system. The program starts with calculating the root mean square (RMS) value of the load current $I_{\rm rms}$ over the past ac cycle in a rolling basis, followed by calculating the accumulated transmitted energy $E_{\rm sum}$ over a preset rolling time window. If the accumulated energy $E_{\rm sum}$ exceeds a preset threshold $E_{\rm max}$, it is deemed to be an overload fault, and the FAULT_TYPE flag will be set to OVERLOAD before the program returns to the fault detection program, where an overload protection program will be activated and the MOSFETs will be turned OFF at the next ac voltage zero-crossing.

### C. Ground Fault Protection Strategy

A ground fault detection program will calculate the RMS value of the ground current $\rm I_{GF\text{-}RMS}$ over one full cycle (16.7 ms for 60 Hz ac) on a continuous rolling basis during each timer interrupt cycle. If $I_{\rm GF\text{-}RMS}$ exceeds 5 mA, it is deemed to be a ground fault, and the FAULT_TYPE flag will be set to GROUND_FAULT before the program returns to the fault detection program, where a ground fault protection program will be activated and the MOSFETs will be turned OFF at the next voltage zero-crossing.

## IV. Arc Fault Protection Method

Smart Plug 2.0 needs to protect against series arc faults originated from partially broken wires, worn out switches, faulty relays, or other forms of poor electrical connections. For example, loosened electrical connections due to vibration over

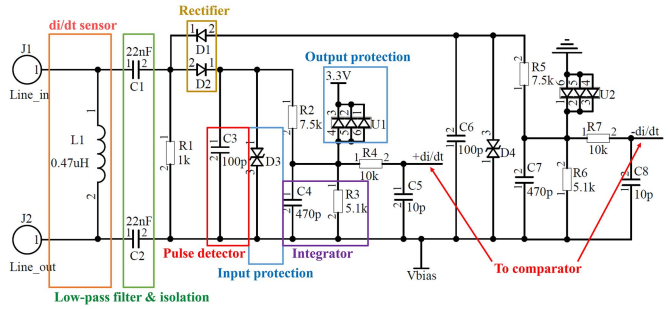


Fig. 7. Arc fault di/dt event detection circuit schematic.

time, improperly installed connections, severed conductors with intermittent continuity, or carbon-based contamination around the exposed conductors can all induce series arcs and cause fire hazards [17]. In this section, a new arc fault protection method is introduced. The proposed method detects and isolates series arc faults before they become dangerous and prevent fire hazards in homes and offices. The method is based on sensing abrupt changes or glitches of the load current (referred to as *di/dt* events in this article). First, a *di/dt* event detection circuit is introduced. Then, the detection strategy is explained, followed by its implementation based on a machine learning method.

### A. Arc Fault Detection Circuit

The proposed arc fault detection method requires an analog *di/dt* event detection circuit to sense abrupt changes in the load current as a result of poor electrical connection or series arc. The circuit schematic of the *di/dt* event detection circuit is shown in Fig. 7. An inductor is connected in series with the line wire. The voltage induced across the inductor is proportional to the inductor current rate of change

$$U = L\frac{di}{dt} \tag{3}$$

where $U$ is the self-induced voltage across the inductor, $L$ is the inductance value, and *di/dt* is the inductor current rate of change.

Arc fault detection concepts were previously proposed to use an inductor or the primary winding of a transformer to monitor the *di/dt* in the ac line wire and integrate the *di/dt* signals within a time window [18], [19]. However, the *di/dt* signals are processed differently to identify an arc fault in this article. The overall arc fault detection circuit combines the use of both analog and digital circuits. According to (3), the sensitivity of the analog *di/dt* detection circuit is determined by the inductor $L1$. Capacitors $C1$ and $C2$ form a high pass filter/isolator to pass the high frequency *di/dt* signals and provide voltage isolation. Meanwhile, the capacitors have very small impedance to high frequency *di/dt* signals resulting from arc, which are in a typical range of 1.5–30 MHz [20]. Resistor $R1$ provides a discharge path for the residual energy stored in the components to ensure safety. Input protection TVS diode $D3$ protects the circuit components against excessive voltage across inductor $L1$. Since the ac current across the inductor $L1$ is bidirectional, the *di/dt* signal can be either positive or negative. The *di/dt* event detection circuit splits into two identical parts to capture $+di/dt$ (rising edge) and $-di/dt$ (falling edge) signals, respectively, using diodes $D1$ and $D2$. The $+di/dt$ sensing circuit consists of $D2$, $D3$, $C3$, $C4$, $C5$, $R2$, $R3$, $R4$, and $U1$ while the $-di/dt$ sensing circuit consists of $D1$, $D4$, $C6$, $C7$, $C8$, $R5$, $R6$, $R7$, and $U2$. The operation of the $+di/dt$ capture circuit is explained next.

The *di/dt* pulse detection circuit includes capacitor $C3$ and discharge resistor $R2$. When *di/dt* induces a voltage across $L1$, the magnetic energy in $L1$ is stored as electrostatic energy in $C3$ instantly. The integrator circuit consists of $C4$ and $R3$. $C4$ integrates the stored *di/dt* energy in $C3$. The time constant $\tau_i$ of the integrator circuit determines the time resolution of the *di/dt* detector. For example, $C4$ can be charged by a series of *di/dt* pulses, followed by a time interval $t = \tau_i$ without any *di/dt* pulses. Consequently, the voltage across $C4$ goes to zero. The resulting output of $C4$ is one pulse, whose magnitude and pulsewidth correspond to the total *di/dt* energy and the number of *di/dt* pulses respectively. In this article, a single *di/dt* pulse across the inductor corresponds to one pulse with a width of approximately 5 $\mu$s across $C4$. Output protection diode array $U1$ absorbs the energy from $C4$ when its voltage exceeds the voltage tolerance of the next stage circuit. First order low pass filter consists of $R4$ and $C5$ with a cutoff frequency of 1.59 MHz is used to filter out high frequency noise coupled from the ac line. The output of the *di/dt* pulse detection circuit is connected to a voltage comparator, which generates a time-stamped *di/dt* pulse train to feed the microcontroller, which stores and analyzes the *di/dt* pulse data using the arc fault detection strategy as to be discussed next.

### B. Arc Fault Detection Strategy

It is essential to define the type of arc faults to be protected by Smart Plug 2.0. Arc faults can be categorized as series or parallel type and reproduced in the laboratory environment using parallel point contact, wet arc (saltwater drip), poor contact, carbonized path, and other testing methods [17]. Parallel arc faults usually generate an excessive fault current similar to that of a short circuit fault. UL1699 AFCI standard requires a combination type AFCI circuit breaker in every branch/feeder in new or newly renovated homes to protect against parallel arc faults [21]. Series arc faults, on the other hand, are much more difficult to detect since the fault current is usually below the parallel arc fault current trip point, but nevertheless are equally hazardous. Furthermore, many household appliances, such as power tools, light switches, or dimmers, generate load current glitches similar to those of series arc faults, and potentially cause nuisance tripping [17]. For this reason, most commercial AFCIs do not provide series arc protection [22].

Various arc signatures are used to detect series arc faults in the prior art. Signatures uniquely associated with series arc can be extracted from voltage, current, or non-electrical signals (e.g., light, heat, etc.). It is a common practice in residential applications to extract arc signatures from the load current in frequency or time domain. Frequency domain arc signatures include high frequency energy [18], high frequency noise [19], frequency spectrum [23], and power spectral density [20]. For

example, Yang et al. [20] proposed a machine learning model using power spectrum signatures to detect series arc faults. Time domain signatures include abrupt changes of the load current (*di/dt* events) [18], current amplitude variation [24], current waveform anomaly [23], and chaotic nature of arc currents [22]. For example, Le et al. [24] developed a machine learning model using current amplitude variation as an indicator of series arc faults. Moreover, Müller et al. [23] proposed an arc fault detection method using both frequency spectrum and current waveform features to detect series arc faults.

The aforementioned *di/dt* event detection circuit in Fig. 7 captures the load current glitches by detecting both positive and negative *di/dt* events of the load current. A rolling time window of 0.5 s is selected per UL1699 standard [21] to monitor the time-stamped *di/dt* events. Both load current intermittencies due to poor connection and actual series arcs can generate a series of *di/dt* pulses to be analyzed by the microcontroller. These *di/dt* events will be distributed along the time axis within the rolling time window. Smart Plug 2.0 analyzes the *di/dt* events data by defining two characteristic parameters: the total number of *di/dt* events *n* and the total number of ac cycles containing at least one *di/dt* event *m* (referred to as "noisy ac cycles" in this article) within each rolling detection window that is made of 30 ac cycles. Series arcs usually generate more *di/dt* events than normal operation of household appliances, thus parameter *n* is a good indicator of series arcs. However, *n* alone may be a necessary, but not sufficient criterion for identifying series arcs since some normal load switching or dimmer operation may generate a similar number of *di/dt* events. Therefore, parameter *m*, representing the time distribution of the *di/dt* events across the entire rolling window, is used as a second criterion. For example, normal load switching through a relay generates a relatively large number of *di/dt* events (a large *n*) but mostly within a single ac cycle immediately after the relay action (a small *m*). In contrast, an arc-inducing poor electrical connection generates a large *n* and a large *m* (that is, the *di/dt* events randomly spreading out across many "noisy" ac cycles within the 0.5 s rolling window). One tends to stipulate that using the *n* and *m* characteristic parameters can effectively distinguish between normal loads and arc faults. However, due to the vast variety of household loads and their diverse behaviors, and the random and chaotic nature of bad electrical connections, using fixed *n* and *m* arc fault thresholds may lead to either nuisance tripping or no response to a true arc fault. In addition, as the load current $I_{\mathrm{load}}$ increases, flame starts sooner from a carbonized path. When the load current is less than 3 A, the arc energy is less than the electrical energy due to incandescence and is insufficient to ignite the cable. When the load current exceeds 10 A, flame can start without carbonized path, and the two broken conductors could be wielded together [25]. The probability of flames outbreak as a function of load current is experimentally measured in [25]. Flame outbreak is most likely to happen between 3 and 10 A. Therefore, the *n* and *m* arc fault thresholds need to be adjusted according to the load current, making the arc fault detection extremely complex and difficult. As a result, a machine learning based detection method is introduced next to determine an arc fault using all three parameters of *n*, *m,* and $I_{\mathrm{load}}$.

### C. Machine Learning-Based Arc Fault Detection

Support vector machine (SVM) is a popular machine learning method widely used in bioinformatics due to its high accuracy in classifying high-dimensional data [26]. In this article, data points are separated into two classes: the arc fault group and normal load group. SVM then creates a decision boundary which best separates the data points by learning to correctly classify the classes. To minimize nuisance tripping, the decision boundary should be drawn as far away from both classes as possible. What's unique about support-vector machine is the way it chooses the decision boundary that maximizes the distance from the nearest data points of both classes. SVM is also known as maximum margin classifier. Therefore, SVM is selected over other machine learning models.

The data set is labeled based on the experiment condition of each data point. Due to the limited normal load samples, $I_{\mathrm{load}}$ only has five discrete values: 2; 4; 6; 8; and 10 A in this article. For the data points labeled as "normal load," the experiments are conducted using a variety of household or office appliances under normal operation, such as resistive type loads (water kettle and space heater), nonlinear type loads (thyristor-type light dimmer and LED light), inductive type loads (handheld power tools and vacuum cleaner), and combined-type loads (hair dryer and microwave oven).

On the other hand, "arc fault" data points are generated by emulating poor electrical connection, which is a major cause of series arc faults. It is conventionally simulated in the laboratory environment using the point contact arc test method, in which two electrodes are controlled to make and break in different speeds. The arc generator consists of a static graphite rod electrode and a moving copper rod electrode. The moving electrode is mounted in a slider and driven into contact with the static electrode by a stepper motor [21]. In this article, a similar arc generator is used, which consists of a fixed 14 AWG wire and a moving 14 AWG wire, both being stripped with metal strands exposed. The moving wire is rotated in contact with and away from the fixed wire by a rotary knob. The two conductors make contact and separate rapidly in a random manner to reflect the chaotic nature of arc faults [22]. The poor connection and arc faults SVM data samples are generated using this method at five load current levels of 2, 4, 6, 8, and 10 A using different load resistors. A total of 300 samples are collected with an observation time window of 0.5 s. At each current level, there are 30 samples from poor connection or arc faults and another 30 samples from normal load operation. The parameters *n*, *m,* and $I_{\mathrm{load}}$ are extracted from each sample using MATLAB and labeled as arc fault or normal load. As a result, a 3-D (*n*, *m,* and $I_{\mathrm{load}}$) feature space is constructed in the form of five 2-D (*n* and *m*) feature spaces to provide training dataset for each load current level, as is shown in Fig. 8.

Fig. 9 shows the arc fault detection program flowchart based on the SVM machine learning model. First, the program will count the total number of *di/dt* events (*n*) and noisy cycles (*m*) in a 0.5 s rolling window. Then, it will calculate the average load current $\mathrm{I_{load\text{-}AVG}}$ within the same 0.5 s rolling time window. According to the value of $I_{\mathrm{load\text{-}AVG}}$, a corresponding SVM

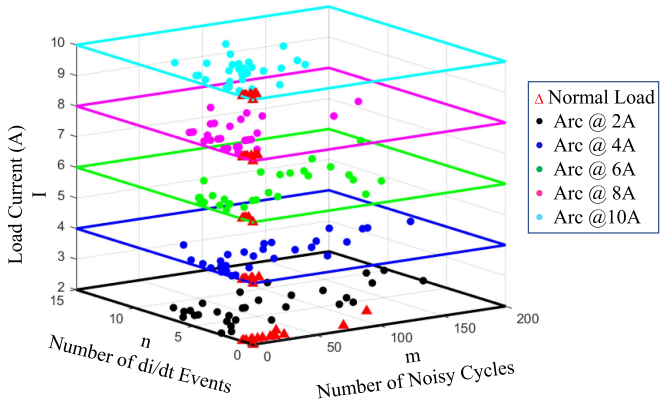


Fig. 8. Trained arc faults predictive SVM models using three characteristic parameters: number of *di/dt* events (*n*), number of noisy cycles (*m*), load current (*I*). The load current variable has five discrete values: 2; 4; 6; 8; and 10 A. The 3-D model consists of five 2-D SVM models stacked along the *I*-axis. The 2-D SVM models correspond to a load current range. For example, the 10 A SVM model, which sits on "10" on the *I*-axis, corresponds to load current of 8–10 A. The triangles are normal load samples, and the arc fault samples are circles corresponding to their respective 2-D SVM models.

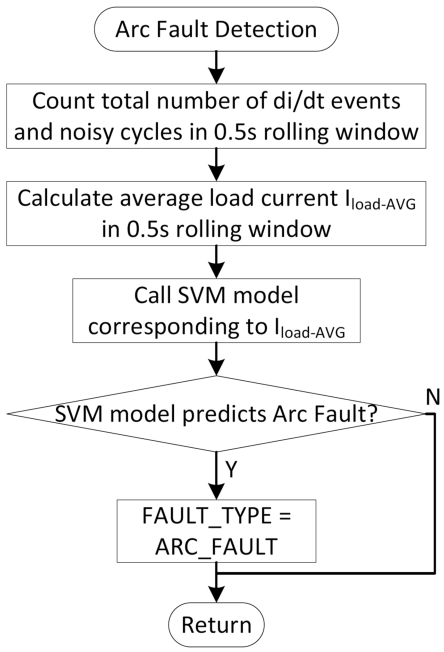


Fig. 9. Arc fault detection program flowchart based on machine learning method.

model is called to predict if an arc fault is present based on *n*, *m,* and $I_{\text{load-AVG}}$. If the model determines that arc fault is present, the FAULT_TYPE flag will be set to ARC_FAULT before the program returns to the fault detection program, where an arc fault protection program will be activated and the MOSFETs will be turned OFF at the next voltage zero-crossing.

## V. Experimental Results

A 120 V/10 A Smart Plug 2.0 prototype is designed and built to demonstrate the comprehensive protection functions previously discussed, as shown in Fig. 10. Hardware component details and

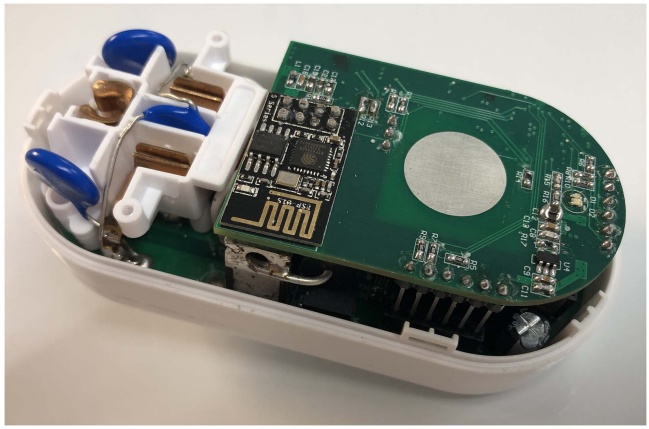

Fig. 10. Actual photo of the Smart Plug 2.0 prototype.

TABLE II
Major Hardware Components List

| Component | Mfg. Part Number | Quantity |
|---|---|---|
| Microcontroller | STM32L432 | 1 |
| Power MOSFET | IXFP80N25X3 | 2 |
| MOSFET gate driver | SI8271GB-IS | 1 |
| Hall effect current senor | ACS733KLATR-40AB | 1 |
| Wi-Fi module | ESP01 | 1 |
| Temperature sensor NTC | NCU18XH103F60RB | 1 |
| *di/dt* sensor inductor | 744314047 | 1 |
| Ground fault sensor | INA826AIDR | 1 |
| Over-voltage MOV | B72214P2151K101 | 3 |
| Voltage sensor amplifier | LMV358AIDGKR | 1 |

experimental results as well as the arc fault detection machine learning model performance evaluation are discussed in this section.

The major hardware components used in this design are given in Table II. An STM32L432 microcontroller is used in the Smart Plug 2.0 prototype. Two power MOSFETs rated 250 V/80 A/16 mΩ (IXYS IXFP80N25X3) are used in a back-to-back configuration, offering a total on-resistance of 32 mΩ. The Smart Plug 2.0 has a maximum power dissipation of 3.2 W at full load and does not need any heat sink. The MOSFET gate driver is an isolated driver IC from Silicon Lab (SI8271GB-IS). A bidirectional Hall effect current senor (ACS733KLATR-40AB) is used to monitor the load current with a response time of 200 ns. A 4.7 $\mu$H inductor is used as the *di/dt* sensor for detecting arc faults. An analog signal processing circuit processes the *di/dt* signals and sends the resulting time-stamped *di/dt* pulse train to the microcontroller. The ground fault current sensor is a differential current transformer with the line and neutral wires going through the center of a small ferrite core. An amplifier circuit is used to amplify this signal before sending it to the Adc of the microcontroller. A low-cost commercial Wi-Fi module ESP01 is used to provide Wi-Fi communication.

Fig. 11 shows the measured load current and MOSFET gate driver signal waveforms under an overload condition. The overload threshold is set to be $9.7\text{A}_{\text{RMS}}$ in this experiment. If the continuously monitored electric energy transferred over a rolling window exceeds a preset maximum energy (similar to the $I^2t$

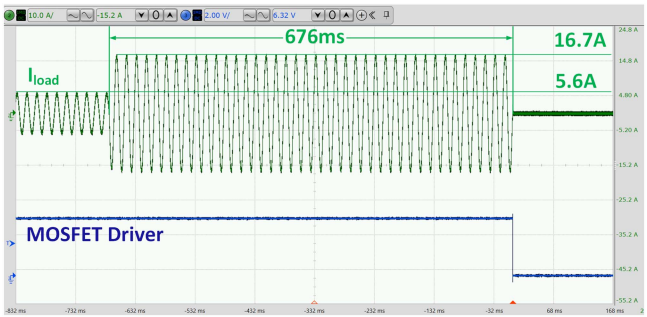


Fig. 11. Measured load current waveforms of Smart Plug 2.0 under an overload condition. The initial load current is at $5.6A_{peak}$ or $4.0A_{RMS}$ when an overload current of $16.7A_{peak}$ or $11.8A_{RMS}$ occurs. The Smart Plug 2.0 shuts down after 0.676 s.

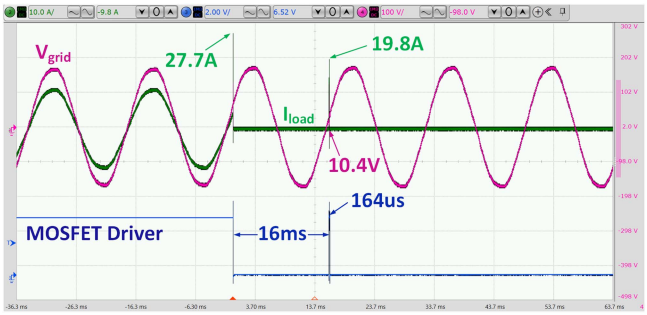


Fig. 12. Measured load current, outlet voltage, and MOSFET driver voltage waveforms under a short circuit fault condition. A peak fault current of 27.7 A is detected and the MOSFETs are turned OFF immediately. After a full half ac cycle, the MOSFETs are "reclosed" at the first voltage zero-crossing. After the fault current reaches 19.8 A again, a short circuit fault is authenticated and the MOSFETs turn OFF permanently.

overload response of a mechanical circuit breaker), the Smart Plug 2.0 turns OFF. It is observed that a resistive load (an electric kettle) with a current of $4A_{RMS}$ is present initially, and then another resistive load of $7.8A_{RMS}$ is added in parallel. The total load current now becomes $11.8A_{RMS}$. The Smart Plug 2.0 shuts down after the overload condition sustains for 676 ms. Note that the power MOSFETs are programed to be turned OFF at the next voltage zero-crossing point to minimize the need to absorb the inductive energy in the circuit loop. This is the preferred operation for the Smart Plug 2.0 except for the instantaneous trip.

Fig. 12 shows the measured load current, outlet voltage, and MOSFET gate driver waveforms under a short circuit fault condition. An electric kettle is initially connected to provide a nominal load current of $7.8A_{RMS}$. A 0.5 Ω resistor is then connected in parallel to emulate a short circuit fault. A peak fault current of 27.7 A is then detected and the MOSFETs are turned OFF immediately by the analog control circuit. After a full half ac cycle, the MOSFETs are "reclosed" at the first voltage zero-crossing by the microcontroller. After the fault current reaches 19.8 A again, a short circuit fault is authenticated and the MOSFETs are turned OFF permanently. It is shown that the MOSFETs are turned ON for 164 $\mu$s during reclosing and fault authentication process.

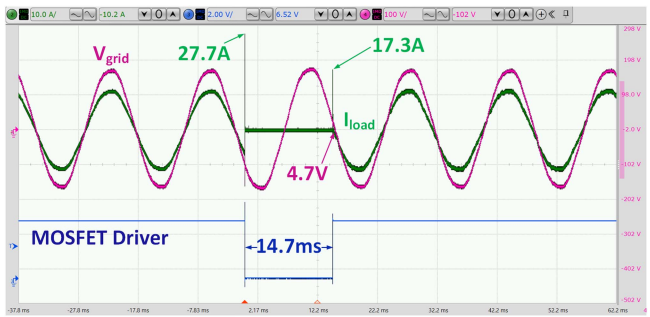


Fig. 13. Measured load current, outlet voltage, and MOSFET driver voltage waveforms under an inrush current condition. The MOSFETs are turned OFF upon detecting a peak inrush current of 27.7 A, but no more overcurrent is detected during the "reclosing" fault authentication process. The MOSFETs remain on afterwards.

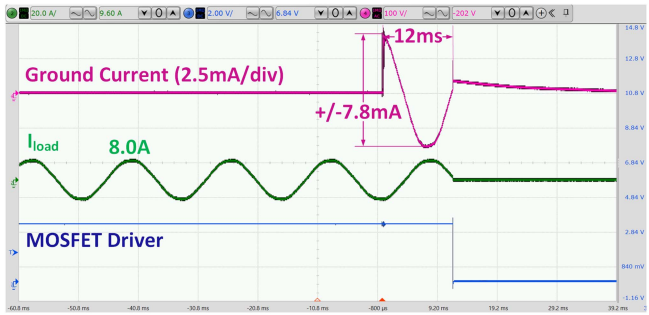


Fig. 14. Measured voltages across the grounding resistor, load current, and MOSFET driver voltage waveforms under a ground fault condition. A normal load current of 8.0 $A_{RMS}$ is present when a grounding resistor of 20.02 kΩ is purposely inserted between the line and ground wires to emulate a ground fault condition. The ground leakage current reaches a peak value of 7.8 mA or 5.5 $mA_{RMS}$. The Smart Plug 2.0 turns OFF the power MOSFETs after a full half ac cycle at the next voltage zero-crossing point.

Fig. 13 shows the measured load current, outlet voltage, and MOSFET gate driver waveforms under an inrush current condition. At first, the electric kettle is present with a nominal load current of $7.8A_{RMS}$. Then, a 20 $\mu$F capacitor is connected in parallel with the load to induce an inrush current to emulate the startup situation of charging the input capacitor of a load. The sudden connection of the capacitor causes a peak inrush current of 27.7 A and the Smart Plug 2.0 turns OFF the power MOSFETs within a few microseconds. When the Smart Plug 2.0 runs its fault authentication program next, the MOSFETs are turned ON at the first zero-crossing point after a full half ac cycle. This time the capacitor is partially charged and continues charging from zero voltage and does not induce a high inrush current. The Smart Plug 2.0 therefore remains in the on state afterwards. It is observed that the Smart Plug 2.0 prototype can distinguish between a high inrush current and a true short circuit fault current.

Fig. 14 shows the measured voltage across the grounding resistor, load current, and MOSFET driver voltage waveforms under a ground fault condition. A normal load current of $8A_{RMS}$ is present when a shorting resistor of 20.02 kΩ is purposely inserted between the line and ground wires to emulate a ground

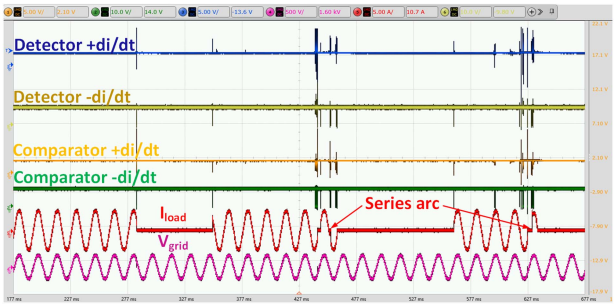


Fig. 15. Measured $+di/dt$ and $-di/dt$ signals from the output of the arc fault detection circuit (detector), $+di/dt$ and $-di/dt$ signals from the output of the comparator circuit (comparator), load current, and outlet voltage waveforms under poor connection and series arc fault conditions. The time window shown is 0.5 s. A normal load current of $2A_{RMS}$ is present when broken ac line wires contact and separate rapidly to emulate a poor connection condition. The current shoulders are typical series arc current waveform.

fault condition. The microcontroller turns OFF the power MOSFETs after a full half ac cycle at the next voltage zero-crossing upon detecting a ground fault current greater than $5mA_{RMS}$.

Fig. 15 shows the $+di/dt$ and $-di/dt$ signals from the arc fault detection circuit and the voltage comparator circuit, load current, and outlet voltage waveforms under poor connection and series arc fault conditions. A resistive load current of $2A_{RMS}$ is present when the broken ac line conductors make contact and separate rapidly to emulate a poor connection condition. It is observed that the *di/dt* events occur at the time of contacting and separation of the two conductors, as well as when series arcs extinguish and re-ignite. The typical series arc current signature waveform is observed, which occurs at the load current shoulder near current zero crossings [23]. The densely distributed *di/dt* events near the current shoulder indicate the presence of series arcs. On the other hand, intermittent contacts and separation generate less *di/dt* signals than the series arc, similar to normal load switching using a relay.

To develop a machine learning model that can distinguish between normal load and poor connection or series arc, based on parameters $n$, $m$, and $I_{load}$, the dataset mentioned in Section IV is used to train and validate the model using MATLAB classification learner App, which makes it easy to select training dataset, specify validation schemes, train models with different types of SVM, and compare the results using different SVMs. Although validation dataset is not used to train the model and is used to validate the model predictive accuracy compared to training dataset, cross-validation is used to fully utilize the dataset. A re-sampling procedure is used in model training to make use of all the data [27]. In this article, a five-fold cross-validation is used. The whole dataset is randomly re-ordered and generates five splits of training and validation sets. For each split of dataset, the training set is used to train the model while the validation set is used to evaluate the model. Then, model is trained and evaluated five times with all five splits, and the accuracy of the model is the average.

To illustrate the effectiveness of the SVM model, the 2 A load current dataset is used to train SVM models. The comparison of the predictive accuracy of different types of trained SVM model

TABLE III
PREDICTIVE ACCURACY COMPARISON OF SVM MODELS

| SVM Model Type | Accuracy |
|---|---|
| Linear | 76.70% |
| Quadratic | 98.30% |
| Cubic | 96.70% |
| Fine Gaussian | 96.70% |
| Medium Gaussian | 93.30% |
| Coarse Gaussian | 76.70% |

TABLE IV
CONFUSION MATRIX OF THE QUADRATIC SVM MODEL

| | | Predicted Class | | |
|---|---|---|---|---|
| | | Arc | Normal | Total |
| True Class | Arc | **30** | 0 | 30 |
| | Normal | 1 | **29** | 30 |
| | Total | 31 | 29 | |

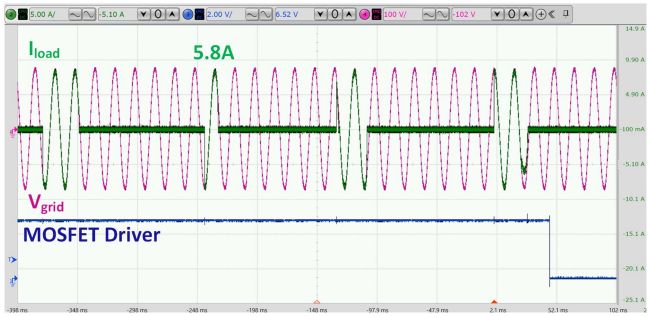


Fig. 16. Measured load current, outlet voltage, and MOSFETs driver voltage waveforms under a poor connection condition. A normal load current of $5.8A_{RMS}$ is present when broken ac line wires contact and separate rapidly to emulate a poor connection condition. The wires contact and separate four times in 0.5 s. The Smart Plug 2.0 turns OFF the power MOSFETs at the next voltage zero-crossing point when the machine learning model predicts arc fault condition is present within the 0.5 s rolling window.

is shown in Table III, the accuracy of Quadratic SVM has the highest accuracy of 98.3%. As is demonstrated in [26], nonlinear SVM provides better accuracy. The confusion matrix in Table IV describes the performance of the model, the diagonal values in bold number show the number of samples being correctly classified. All five SVM models corresponding to each current level are trained and selected in the same manner. The resulting 3-D SVM model is demonstrated in Fig. 8. The red triangle data points in Fig. 8 are classified as normal load, while others are classified as arc fault. As a result, the model could be programmed in the microcontroller. In machine learning, a test dataset is used to evaluate the model once a model is completely trained. It should contain data that covers most scenarios the model would face in the real world. Therefore, the model is tested using Smart Plug 2.0 prototype under household loads and arc fault or poor connection conditions. The results show that the model can detect 100% of the arc faults in a reasonable number of experiments.

Fig. 16 shows the measured load current, outlet voltage, and MOSFET gate driver waveforms under a poor connection

condition. The line wire of the load is severed, and poor connection condition is simulated using the method described in Section IV. At first, a small heater with a current of $5.8A_{RMS}$ is present when the broken ac line wires start to contact and separate rapidly. The wires contact and separate roughly four times within the 0.5 s time window. Smart Plug 2.0 calculates and average the load current RMS value every half ac cycle. If incomplete half cycle is present, only the nonzero values are used in averaging. Then, an SVM model corresponding to the calculated load current level is used to predict if arc fault condition is present in the 0.5 s rolling window. If arc fault condition is confirmed, Smart Plug 2.0 turns OFF the power MOSFETs at the next voltage zero-crossing point.

## VI. Conclusion

Smart plug devices offer a cost-effective way to automate homes, restaurants, hotels, and other businesses, and can easily enable the demand response concept for improving energy efficiency. Conventional Smart Plug products on the market, however, do not offer any protection against fire or shock hazards commonly caused by degraded power cords and electrical connections.

This article introduces a new Smart Plug 2.0 concept which provides comprehensive protection and prevents fire and shock hazards caused by degraded or damaged power cords and electrical connections in homes and offices in addition to the wireless power ON/OFF function offered by the Smart Plug 1.0 products on the market today. Smart Plug 2.0 can also distinguish between a dangerous arc fault and normal load operation, using a machine learning model prediction method. The basic concept and control algorithms of the Smart Plug 2.0 are discussed in this article. A 120 V/10 A Smart Plug 2.0 prototype is built using cost-effective microcontroller, Wi-Fi module, silicon power MOSFETs, various sensors, and other components. A new arc fault detection method is developed, and a highly accurate machine learning model is validated experimentally. The intended Smart Plug 2.0 protective functions under overload, short circuit, inrush startup conditions, ground fault, and arc fault are experimentally demonstrated. Note that our proposed design method allows the integration of all the protective functions by sharing the same basic hardware platform with minimal cost penalty, a distinctive feature from other solid state circuit breaker designs. Future work includes development of user-friendly mobile applications, integration into smart home eco-systems, optimization of circuit fault protection algorithms, and commercialization of the prototype.

## Acknowledgment

The views and opinions of authors expressed herein do not necessarily state or reflect those of the United States Government or any agency thereof.

## References

[1] R. Campbell, "Home electrical fires," Nat. Fire Protection Assoc., Quincy, MA, USA, Mar. 2019. [Online]. Available: https://www.nfpa.org/News-and-Research/Data-research-and-tools/Electrical/Electrical
[2] J. Rey et al., "How arc fault detection devices minimize electrical fire threats," Schneider Elect., Le Creusot, France, 2017. [Online]. Available: https://www.se.com/ww/en/download/document/EDCED117020EN/
[3] "Home electrical fires," Elect. Saf. Found. Int., 2022. [Online]. Available: https://www.esfi.org/home-electrical-fires/
[4] "Overload or short circuit protection? How to protect your design against both dangers," E-T-A Elektrotechnische Apparate GmbH, IL, USA, 2021. Accessed: Mar. 20, 2021. [Online]. Available: https://www.e-t-a.co.uk/resources/white_papers/overload_or_short_circuit_protection_how_to_protect_your_design_against_both_dangers/
[5] "Understanding ground fault and leakage current protection," Jan. 2009. [Online]. Available: https://code-authorities.ul.com/wp-content/uploads/2014/04/ul_GroundFaultProtectiveDevices.pdf
[6] "Global smart plug market 2017-2021," Infiniti Res. Ltd., IL, USA, 2020. Accessed: Apr. 4, 2020. [Online]. Available: https://www.technavio.com/report/global-consumer-electronics-globalsmart-plug-market-2017-2021
[7] P. Mtshali and F. Khubia, "A smart home energy management system using smart plugs," in *Proc. Conf. Inf. Commun. Technol. Soc.*, 2019, pp. 1–5.
[8] W. Elmenreich and D. Egarter, "Design guidelines for smart appliances," in *Proc. 10th Int. Workshop Intell. Solutions Embedded Syst.*, 2012, pp. 76–82.
[9] J. Kwac, J. Flora, and R. Rajagopal, "Household energy consumption segmentation using hourly data," *IEEE Trans. Smart Grid*, vol. 5, no. 1, pp. 420–430, Jan. 2014, doi: 10.1109/TSG.2013.2278477.
[10] Z. Shen, Z. Deng, and Y. Zhou, "Solid state protective smart plug device," U.S. Patent US2022/0029362 A1, Jul. 27, 2020.
[11] Z. Deng, Y. Zhou, R. Na, and Z. J. Shen, "Smart plug 2.0: Solid state smart plugs preventing fire and shock hazards in smart homes and offices," in *Proc. IEEE Energy Convers. Congr. Expo.*, 2020, pp. 6065–6070, doi: 10.1109/ECCE44975.2020.9235862.
[12] O. Elma and U. S. Selamoğullari, "A home energy management algorithm with smart plug for maximized customer comfort," in *Proc. 4th Int. Conf. Elect. Power Energy Convers. Syst.*, 2015, pp. 1–4.
[13] M. B. Satti, N. Ali, M. M. A. Asif, A. H. Abid, and A. Hasan, "A low-cost smart load enabler device," in *Proc. 15th Int. Conf. Smart Cities: Improving Qual. Life Using ICT IoT*, 2018, pp. 61–64.
[14] "Circuit breaker characteristic trip curves and Coordination," Schneider Elect., Cedar Rapids, IA, USA, 2018. [Online]. Available: https://www.se.com/us/en/download/document/0600DB0105/
[15] Y. Zhou, Y. Feng, and Z. J. Shen, "iBreaker: Intelligent Tri-mode solid state circuit breaker technology," in *Proc. IEEE Int. Power Electron. Appl. Conf. Expo.*, 2018, pp. 1–7, doi: 10.1109/PEAC.2018.8590629.
[16] Y. Zhou, Y. Feng, T. Liu, and Z. J. Shen, "Short circuit fault location in DC power network using intelligent SiC solid-state circuit breaker," in *Proc. IEEE Energy Convers. Congr. Expo.*, 2018, pp. 485–491, doi: 10.1109/ECCE.2018.8557923.
[17] T. E. Potter, "Arc fault interruption requirements for aircraft applications," Texas Instrum., Dallas, TX, USA, Nov. 2003.
[18] S. J. Brooks, J. W. Dickens, and W. Strader, "Arcing fault detection system," U.S. Patent 6195241B, Feb. 27, 2001. [Online]. Available: https://patents.google.com/patent/US6195241B1
[19] C. V. Pellon et al., "Apparatus and method for detecting arc faults," European Patent 1638181B1, Aug. 15, 2012. [Online]. Available: https://patents.google.com/patent/EP1638181B1
[20] K. Yang, R. Zhang, J. Yang, C. Liu, S. Chen, and F. Zhang, "A novel Arc fault detector for early detection of electrical fires," *Sensors*, vol. 16, no. 4, 2016, Art. no. 500.
[21] *Standard for Safety for Arc-Fault Circuit-Interrupters*, UL1699, 2017.
[22] J. C. Engel, "Combination AFCIs: What they will and will not do," in *Proc. IEEE IAS Elect. Saf. Workshop*, 2012, pp. 1–18, doi: 10.1109/ESW.2012.6165548.
[23] P. Müller, S. Tenbohlen, R. Maier, and M. Anheuser, "Characteristics of series and parallel low current arc faults in the time and frequency domain," in *Proc. Proc. 56th IEEE Holm Conf. Elect. Contacts*, 2010, pp. 1–7, doi: 10.1109/HOLM.2010.5619539.
[24] V. Le, X. Yao, C. Miller, and B. Tsao, "Series DC arc fault detection based on ensemble machine learning," *IEEE Trans. Power Electron.*, vol. 35, no. 8, pp. 7826–7839, Aug. 2020, doi: 10.1109/TPEL.2020.2969561.

[25] "Application manual—Arc fault detection devices AFDD," OEZ s.r.o., Letohrad, Czech Republic, 2017. Accessed: Sep. 1, 2021. [Online]. Available: https://flameport.com/electrical_theory/AFDD_arc_fault_device/mi02_2017_en.pdf
[26] A. Ben-Hur and J. Weston, "A user's guide to support vector machines," in *Data Mining Techniques For the Life Sciences. Methods in Molecular Biology (Methods and Protocols)*, vol. 609, O. Carugo and F. Eisenhaber, Eds., Totowa, NJ, USA: Humana Press, 2010.
[27] Y. Wang, L. Hou, K. C. Paul, Y. Ban, C. Chen, and T. Zhao, "ArcNet: Series AC arc fault detection based on raw current and convolutional neural network," *IEEE Trans. Ind. Inform.*, vol. 18, no. 1, pp. 77–86, Jan. 2022, doi: 10.1109/TII.2021.3069849.

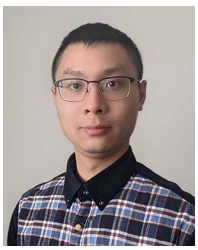

**Zhixi Deng** (Member, IEEE) received B.S. degree in electrical and electronics engineering from the Guangdong University of Technology, Guangzhou, China, in 2016, and the M.S. and Ph.D. degrees in electrical engineering from the Illinois Institute of Technology, Chicago, IL, USA in 2018 and 2022, respectively.

He is currently with Eaton Corporation, Moon Twp, PA, USA, as a Senior Power Electronics Engineer. His main research interests include power electronics, electronic components and circuits, and their applications in circuit breakers.

**Yuanfeng Zhou** (Member, IEEE) received the B.S. degree in electrical engineering from Xi'an Jiaotong University, Xi'an, China, in 2009, the M.S. degree in electrical engineering from the Huazhong University of Science and Technology, Wuhan, China, in 2012, and the Ph.D. degree in electrical engineering from the Illinois Institute of Technology, Chicago, IL, USA, in 2021

From 2012 to 2015, he was with Emerson Network Power, Shenzhen, China, as a Design Engineer. He is currently with Monolithic Power Systems, Kirkland, WA, USA. He has published several articles on these topics. His research interests include dc circuit breakers and dc/dc converters.

**Ahmad Kamal** (Member, IEEE) received the B.S. degree in electrical power engineering from Comsats University, Abbottabad, Pakistan, in 2013, the M.S. degree in electrical energy systems engineering from the University of Engineering and Technology, Peshawar, Pakistan, in 2017, and the Ph.D. degree in electrical engineering from the Illinois Institute of Technology, Chicago, IL, USA, in May 2022.

He has authored and coauthored several papers on these topics. His research interests include Dc solid-state circuit breakers, EV drivetrain, and wide bandgap power electronics.

**Risha Na** (Member, IEEE) received the Ph.D. degree in electrical engineering from the Harbin University of Science and Technology, Harbin, China, in 2013.

In 2013, he was an Assistant Professor with the Department of Electrical and Electronic Engineering, Harbin University of Science and Technology. He was a Senior Research Associate with The Ohio State University, from 2016 to 2019. He is currently a Research Associate Professor with Illinois Institute of Technology, Chicago, IL, USA. His research interests include power electronics and applications of WBG devices in medium-voltage drive systems.

**Ian P. Brown** (Senior Member, IEEE) received the B.S. degree in engineering from Swarthmore College, Swarthmore, PA, USA, in 1999, and the M.S. and Ph.D. degrees in electrical engineering from the University of Wisconsin, Madison, WI, USA, in 2003 and 2009, respectively.

Since 2012, he has been with the Illinois Institute of Technology. Previously, he was with the Corporate Technology Center, A. O. Smith Corporation, Milwaukee, WI, USA. His main research interests are high-performance electrical drives, the design of electric machines, and power electronics.

**Z. John Shen** (Fellow, IEEE) received the B.S. degree from Tsinghua University, Beijing, China, in 1987, and the M.S. and Ph.D. degrees from Rensselaer Polytechnic Institute, Troy, NY, USA, in 1991 and 1994, respectively, all in electrical engineering. Between 1994 and 1999, he held a variety of positions including a Senior Principal Staff Scientist with Motorola. He was the Faculty of the University of Michigan-Dearborn, between 1999 and 2004, the University of Central Florida, between 2004 and 2012, and Illinois Institute of Technology, between 2013 and 2021. He was a Board Member and the Chief Scientist of GWS Semiconductor (now a division of Renesas Electronics), between 2002 and 2012, responsible for developing high-frequency power MOSFET technology for supercomputer and server applications. He was a Professor with Simon Fraser University in Canada and the Director of the School of Mechatronic Systems Engineering in January 2022. He has authored or coauthored more than 300 journal and conference articles, and holds 18 issued U.S. patents in these areas. His research interests include power electronics, power semiconductor devices and ICs, automotive electronics, renewable and alternative energy systems, microgrid, and electronics manufacturing.

Dr. Shen is the recipient of the 2012 IEEE Region 3 Outstanding Engineer Award, the 2003 NSF CAREER Award, the 2006 IEEE Transaction Paper Award from IEEE Society of Power Electronics, the 2003 IEEE Best Automotive Electronics Paper Award from IEEE Society of Vehicular Technology, and the 1996 Motorola Science and Technology Award. He has been an active Volunteer in the IEEE Power Electronics Society, and has served as VP of Products, AdCom member, the Deputy Editor in Chief of *IEEE Power Electronics Magazine*, the Chair of PELS Distinguished Lecturers Program, an Associate Editor and a Guest Editor in Chief of IEEE TRANSACTIONS ON POWER ELECTRONICS, and IEEE JOURNAL OF EMERGING AND SELECT TOPICS IN POWER ELECTRONICS, the General Chair or technical program chair of several major IEEE conferences including European Conference on Cognitive Ergonomics, International Symposium on Power Semiconductor Devices and ICs, IEEE Conference on Vehicle Power and Propulsion, and Power Electronics Specialist Conference. He is a Fellow of the U.S. National Academy of Inventors.